[논 문] - 비파괴검사학회지
*Journal of the Korean Society for Nondestructive Testing*
*Vol. 32, No. 5 (2012. 10)*

http://dx.doi.org/10.7779/JKSNT.2012.32.5.469

# 여러 종류의 표면 진동원에 대한 연조직에서의 진동 변위 비교

# Comparison of Vibrational Displacements Generated by Different Types of Surface Source in a Soft Tissue

박정만*, 권성재*, 정목근*†

Jeong Man Park*, Sung-Jae Kwon* and Mok-Kun Jeong*†

**초 록** 인체 연조직에서 기계적인 진동의 전달 특성은 조직의 탄성 특성에 의존한다. 연조직의 진동 특성으로부터 암이나 종양을 진단할 수 있기 때문에 진동의 전달 특성에 대한 연구는 중요한 의미를 가진다. 이 논문은 연조직의 표면에 위치하는 여러 형태의 응력 진동원에 의해 연조직 내에 발생되는 변위 패턴을 분석하고 비교하였다. 진동원으로는 수직하중, 접선하중, 그리고 면외전단하중이 고려되었다. 점탄성 단일층에서의 변위에 대한 이론적 표현식을 구하였고, 수치계산은 반공간 및 무한평판조직에서 수행되었다. 그리고 유한크기조직에서의 변위패턴을 유한요소법으로 시뮬레이션하였다. 응력 형태, 진동원 크기 및 주파수, 그리고 경계면이 변위에 미치는 영향이 분석되었다.

**주요용어:** 초음파, 진동, 탄성, 횡파, 연조직

**Abstract** The propagation characteristics of a mechanical wave in human soft tissue depend on its elastic properties. Investigation of these propagation characteristics is of paramount importance because it may enable us to diagnose cancer or tumor from the vibration response of the tissue. This paper investigates and compares displacement patterns generated in soft tissue due to several forms of low-frequency vibration sources placed on a surface. Among vibration sources considered are a normal load, tangential load, and antiplane shear load. We derive analytical expressions for displacements in viscoelastic single layers, and calculate displacement patterns in half space and infinite plate type tissue. Also, we simulate the vibration response of a finite-sized tissue using finite element method. The effects of the type of stress, the size and frequency of vibration sources, and medium boundaries on displacement patterns are discussed.

**Keywords:** Ultrasound, Vibration, Elasticity, Shear Wave, Soft Tissue

## 1. Introduction

Applying low-frequency vibration to soft tissue generates a relatively large amplitude shear wave that propagates in it. Because the characteristics of wave propagation depend on mechanical properties of tissue, measurement of vibration amplitude or wave speed can lead one to detect lesions based on tissue elasticity[1-3]. Techniques for visualizing elasticity by measuring the amount of tissue vibration need a vibration source that can generate a relatively large amplitude shear wave. Shear waves can be generated using several methods, such as employing a surface vibration source[4], or applying an acoustic radiation force so as to

[접수일: 2012. 8. 30, 수정일: 2012. 9. 25, 게재확정일: 2012. 9. 28] *대진대학교 전자공학과, †Corresponding Author: Department of Electronic Engineering, Daejin University, Pocheon 487-711, Kyeonggi, Korea (E-mail: jmk@daejin.ac.kr)

generate them inside tissue[5]. They can also be generated inside tissue without external force applied, for example by a beating heart or pulsating blood vessel[6,7].

In order to generate shear wave, sono-elastography[2,8] or transient elastography [9,10] has used various forms of surface vibration sources. Parker et al.[11] used a normal point source to verify FEM simulation results of displacement patterns, Catheline et al.[12] measured the diffraction field of a point source using transient elastography. Yamakoshi et al.[8] applied vibration to a tissue phantom using a perpendicularly vibrating rectangular plate, and Fu et al.[13] used a long, narrow rectangular rod to obtain a plane strain condition.

By applying a shear load to the surface of a phantom with a short cylindrical rod, Gao et al.[14] obtained displacement images formed by horizontal shear wave. Sandrin et al.[9] proposed using dual cylindrical rod vibrators arranged side by side which were placed on both ends of a transducer array in order to generate a large amplitude shear wave in an imaging region of interest. Shear waves emitted from the dual vibration sources are reinforced constructively in the center region between them, resulting in large axial displacements.

Wu et al.[15] used dual vibration sources consisting of two long metal plates (8 mm×90 mm), similar to the above arrangement, to produce a higher resolution sono-elasticity image. Recently, Wu et al.[16,17], McLaughlin et al.[18], and Hoyt et al.[19] have applied shear stress with a bimorphic piezoelectric transducer, and measured the speed of the generated shear wave by observing its interference pattern. They were able to determine the speed of shear wave by visualizing its propagation with only amplitude images in sonoelastography.

Although much experimental research has been conducted to image the elasticity of tissue specimen and phantom by generating waves with a surface vibration source, there has been relatively little theoretical study of wave generation in tissue. Gao et al.[14] theoretically analyzed the displacement pattern of a shear wave generated in tissue due to a low frequency vibration applied. They considered an attenuating medium that includes hard lesions. Royston et al.[20] obtained an analytical solution to the problem of surface wave generation in a viscoelastic half space due to a normal circular vibrator placed on a surface. They analyzed the change in surface displacement inside tissue as a function of the distance from the vibrator. Timanin[21] and Klochkov[22] obtained theoretical expressions for displacements generated in a multi-layer tissue due to a normal circular source, and examined the change in displacement by varying the thickness of tissue and the size and frequency of the vibration source.

In this paper, we investigated the characteristics of vibration patterns generated in tissue by computing displacements due to various forms of stress-generating vibration sources placed on a surface. Among vibration sources considered were a strip shaped normal load, tangential load, and antiplane shear load.

We derived analytical expressions for displacements in a homogeneous viscoelastic single layer whose one side is fixed. Numerical computations were performed in a half space and single layer using the speed of sound in soft tissue for a low-frequency vibration source, and the characteristics of wave generation according to the type of stress applied were compared. We also analyzed displacement patterns in a finite-sized tissue using FEM simulation.

## 2. Theory

As shown in Fig. 1, we consider a single homogeneous viscoelastic layer of thickness $L$,

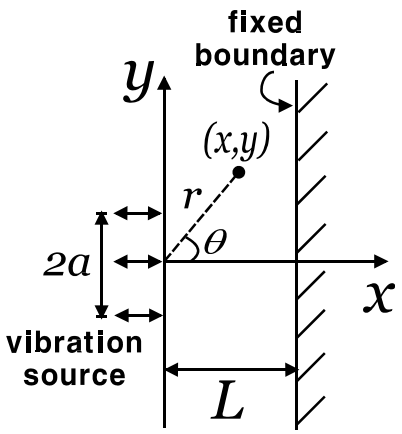


Fig. 1 Coordinate system for the wave generation due to a strip load

which is infinitely extended in the $y$ and $z$ direction. A strip load of width $2a$ is applied to the surface $x=0$, and the surface $x=L$ is fixed.

Assuming linear viscoelasticity, the expression for motion in a viscoelastic medium is the same as that in an elastic medium except that the elasticity coefficient is complex. Thus, the equation of motion in a linear isotropic viscoelastic medium can be written as follows[23]:

$$(\lambda^*+\mu^*)\vec{\nabla}\vec{\nabla}\cdot\vec{u}+\mu^*\nabla^2\vec{u}=\rho\frac{\partial^2\vec{u}}{\partial t^2} \tag{1}$$

where $\vec{u}$ is the displacement vector, $\lambda^*$ and $\mu^*$ are complex Lamé constants, and $\rho$ is the density. Using the Voigt viscoelastic model, we have $\lambda^*=\lambda+i\omega\kappa$ and $\mu^*=\mu+i\omega\eta$. $\kappa$ and $\eta$ are, respectively, longitudinal and shear viscosity coefficients, and $\omega$ is the angular frequency of harmonic oscillation.

### 2.1 Wave Generation from Normal and Tangential Load

If we apply a normal and tangential load to the surface of a medium, a plane-strain oscillation occurs in the medium. In this case, the boundary conditions are

$$x=L,\ u_x=u_y=0, \tag{2}$$

$$x=0,\ \sigma_{xx}=\sigma(y)\,e^{i\omega t},\ \sigma_{xy}=0,\ \text{(case of normal load)}, \tag{3}$$

$$x=0,\ \sigma_{xx}=0,\ \sigma_{xy}=\sigma(y)\,e^{i\omega t},\ \text{(case of tangential load)}, \tag{4}$$

where $\sigma_{pq}(p,q=x \text{ or } y)$ denotes stress components.

A solution to eqn. (1) can be obtained using Fourier transform in an analogous manner to solving a two-dimensional Lamb problem in a half space[24]. Expressing the displacement as the sum of the gradient of scalar potential and the curl of vector potential, we obtain two separate wave equations for longitudinal and shear waves[14,25]. Taking the Fourier transform of the resulting equations in the spatial variable $y$ and taking the inverse Fourier transform of a general solution for the transformed wave equation give the following expression for the displacement component in the medium:

$$u_k(x,y)=\frac{1}{2\pi}\int_{-\infty}^{\infty}\overline{u_k}(x,\xi)e^{i\xi y}d\xi,\ k=x,y \tag{5}$$

where $\overline{u_k}$ represents the Fourier transformed displacement components given as

$$\overline{u_x}(x,\xi)=\alpha(A\cosh\alpha x+B\sinh\alpha x)-\xi(C\sinh\beta x+D\cosh\beta x), \tag{6}$$

$$\overline{u_y}(x,\xi)=i[\xi(A\sinh\alpha x+B\cosh\alpha x)-\beta(C\cosh\beta x+D\sinh\beta x)], \tag{7}$$

Here, $\alpha=\sqrt{\xi^2-\omega^2/[c_l^2(1+i/Q_l)]}$, $\beta=\sqrt{\xi^2-\omega^2/[c_s^2(1+i/Q_s)]}$, $\xi$ is a parameter in the transform, and $c_l=\sqrt{(\lambda+2\mu)/\rho}$ and $c_s=\sqrt{\mu/\rho}$ are, respectively, the speed of the longitudinal and shear waves.

$Q_l=(\lambda+2\mu)/[\omega(\kappa+2\eta)]$ and $Q_s=\mu/\omega\eta$ are, respectively, the acoustic $Q$ of the longitudinal

and shear waves[26]. The corresponding attenuation of the waves in the medium is $\omega/(2c_jQ_j)$, where $j=l,s$. The unknowns, $A$, $B$, $C$, and $D$ in eqns. (6) and (7) are determined by solving a set of linear equations satisfying boundary conditions (2)-(4). The displacement in a half space can be obtained by letting $L\rightarrow\infty$ in the solution to the single layer case. The displacement expressions are identical to the conventional theoretical expressions for an elastic half-space medium except for the complex elastic coefficients[24]. The far field in the region of large $r$ and $0\le\theta<\pi/2$ in a half space can be approximated by integrating the integral expression for the displacement using the steepest-descent method[24]. For the case of a normal load, we obtain the following results for the radial and tangential displacement components:

$$u_r\sim\frac{\sigma_0 e^{i3\pi/4}}{\mu}\left(\frac{2}{\pi r}\right)^{1/2}\frac{k_l^{1/2}\cos\theta\sin(k_l a\sin\theta)(k_s^2-2k_l^2\sin^2\theta)}{\sin\theta F(k_l\sin\theta)}e^{-ik_l r}, \tag{8}$$

$$u_\theta\sim\frac{\sigma_0 e^{i5\pi/4}}{\mu}\left(\frac{8}{\pi r}\right)^{1/2}\frac{k_s^{3/2}\cos\theta\sin(k_s a\sin\theta)(k_s^2\sin^2\theta-k_l^2)^{1/2}}{F(k_s\sin\theta)}e^{-ik_s r}, \tag{9}$$

where $k_l=\omega/c_l$, $k_s=\omega/c_s$, $F(\xi)=(\xi^2+\beta^2)^2$-$4\xi^2\alpha\beta$ and $\sigma_0$ is the magnitude of load. Also, for the case of a tangential load, we obtain the following results:

$$u_r\sim\frac{\sigma_0 e^{i3\pi/4}}{\mu}\left(\frac{8}{\pi r}\right)^{1/2}\frac{k_l^{3/2}\cos\theta\sin(k_l a\sin\theta)(k_s^2-k_l^2\sin^2\theta)^{1/2}}{F(k_l\sin\theta)}e^{-ik_l r}, \tag{10}$$

$$u_\theta\sim\frac{\sigma_0 e^{i3\pi/4}}{\mu}\left(\frac{2}{\pi r}\right)^{1/2}\frac{k_s^{5/2}\cos\theta\cos2\theta\sin(k_s a\sin\theta)}{\sin\theta F(k_s\sin\theta)}e^{-ik_s r}, \tag{11}$$

We can see that from the term $\exp(-ik_l r)$ in eqns. (8) and (10) the component $u_r$ emitted from the strip load propagates at the speed of a longitudinal wave and from the term $\exp(-ik_s r)$ in eqns. (9) and (11) the component $u_\theta$ propagates at the speed of a shear wave.

### 2.2 Wave Generation from Antiplane Shear Load

The antiplane shear stress applied to the surface of a single layer generates only a horizontal shear wave whose displacement component in the medium is $u_z$. Hence, from eqn. (1), the equation of motion is written as

$$\mu^*\nabla^2 u_z=\rho\frac{\partial^2 u_z}{\partial t^2}. \tag{12}$$

The boundary conditions are specified as follows:

$$x=L,\ u_z=0, \tag{13}$$

$$x=0,\ \sigma_{xz}=\sigma(y)e^{i\omega t}. \tag{14}$$

Taking the Fourier transform, solving the wave equations, and imposing the boundary conditions, we obtain the following expression for displacement:

$$u_z(x,y)=\frac{1}{2\pi\mu^*}\int_{-\infty}^{\infty}\frac{\overline{\sigma}(\xi)}{\beta}\left(\sinh\beta x-\frac{\sinh\beta L}{\cosh\beta L}\cosh\beta x\right)e^{i\xi y}d\xi \tag{15}$$

The displacement in a half space due to a strip load of width $2a$ can be expressed in the limit $L\rightarrow\infty$. The displacement expression is the same as plugging in complex elastic coefficients in the conventional theoretical expression in an elastic half space[24]. The far field in an elastic half space is given as

$$u_z\sim\frac{\sigma_0 e^{i3\pi/4}}{u}\left(\frac{2}{\pi r}\right)^{1/2}\frac{\sin(k_s a\sin\theta)}{k_s^{3/2}\sin\theta}e^{-ik_s r}. \tag{16}$$

## 3. Simulation of Vibration in Finite-Sized Tissue

We analyzed the two-dimensional vibration behavior of a finite-sized tissue bounded by the range $-H/2\le y\le H/2$ in Fig. 1 using FEM

simulation. The vibration source is placed at the surface $x=0$ and its center is at $y=0$. The plane $x=L$ is a fixed boundary, and the planes $y=\pm H/2$ are free boundaries.

The damping matrix was constructed from the previous viscous damping, and each viscous coefficient is expressed in terms of the acoustic $Q$ as $\kappa=(\rho/\omega)(c_l^2/Q_l-2c_s^2/Q_s)$ and $\eta=(\rho/\omega)c_s^2/Q_s$. The size of the medium was 4 cm×10 cm, and the entire region was divided into 8,000 six-node triangular elements with 16,281 nodes.

## 4. Numerical Results

The speed of sound in soft tissue was set to $c_l$=1.54×10$^5$ cm/s for longitudinal wave and $c_s$ =290 cm/s for shear wave. These values are within the speed range available in the literature or that in soft tissue estimated from elastic coefficients[1,4,27-30].

### 4.1 Distribution of Displacement in Far Field

In order to examine the characteristics of wave generation due to different types of load, we first computed the displacement in the far field of a half space using eqns. (8)-(11) and (16). The results normalized with respect to $\sigma_0 a/\mu\sqrt{rk_s}$ are presented in Figs. 2-4.

Fig. 2 is a polar plot of the displacement magnitude for a normal and tangential load of width $2a$=0.1 cm and frequency $f(=\omega/2\pi)$ =500 Hz, where $u_r$ and $u_\theta$ denote the displacement components of the longitudinal and shear waves, respectively, and their magnitudes differ from each other greatly. The ratio of the amplitude of the shear wave to that of the longitudinal wave, $|u_\theta|/|u_r|$, for the normal load is asymptotically given as $(c_l/c_s)^{3/2}$, which is on the order of $10^4$, and that for the tangential load as $(c_l/c_s)^{5/2}$, which is on the order of $10^7$. This indicates that even under the normal load, relatively large amplitude shear waves are generated in soft tissue. Accordingly, as can be seen in Fig. 3, the shear wave dominantly contributes to the overall beam pattern. Strong shear waves are generated in specific directions from the normal load, where the angle of maximum displacement in the sidelobe is 32°. For the case of the tangential load, a large amplitude shear wave is emitted in the front of the vibration source. Because $u_\theta$ becomes zero at $\theta=\pm 45^\circ$ due to the term, $\cos 2\theta$, in the numerator of eqn. (11) and the sidelobe levels are small, the shear wave from the tangential load mainly propagates within $|\theta|<45^\circ$ and the angle of maximum displacement is 22.5°. In the case that the width of the vibration source is very small relative to the shear wavelength, the far field due to an antiplane shear source is nearly independent of the angle, and shear waves of similar amplitudes are emitted in all directions in the half space.

Fig. 4 is a polar plot of the displacement profile in the far field due to a vibration source of width 2a=1.0 cm and frequency f=500 Hz. Because the width of the strip load is greater than the wavelength of the shear wave in the medium, the number of sidelobes increases. We can see that the angular width over which the shear wave is strongly emitted has been narrowed compared to Fig. 3. The angles at which the displacement becomes zero between the sidelobes of the shear wave are determined by the expression, $\sin(k_s a\sin\theta)=0$, in eqns. (9), (11), and (16). For regions where $\theta>0$, those angles are given as $\sin\theta_n=nc_s/2af$, where $n=1,2,3,\ldots$. For tangential load, we have an additional angle, 45°, from $\cos 2\theta=0$. When 2a=1.0 cm and f=500 Hz, the null point for the case of the normal and antiplane shear load can be clearly seen at $\theta_1$=35.45°. For the case of the tangential load, the displacements of the shear wave become zero at angles of 35.45° and 45°. Thus, actually there exist a total of four

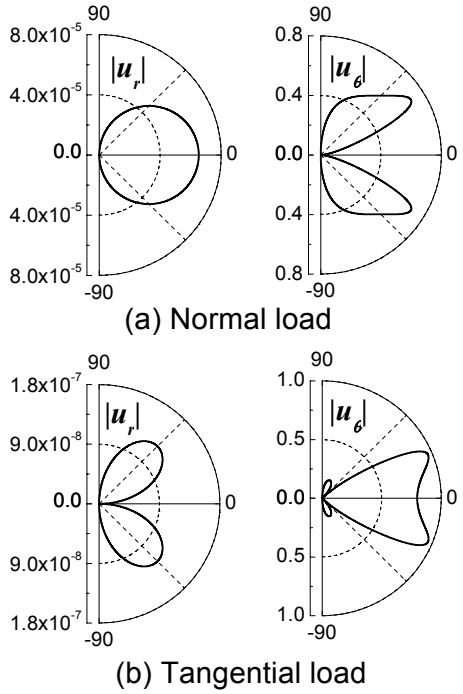


Fig. 2 Polar plots of displacement magnitude in far field for 2a=0.1 cm and f=500 Hz

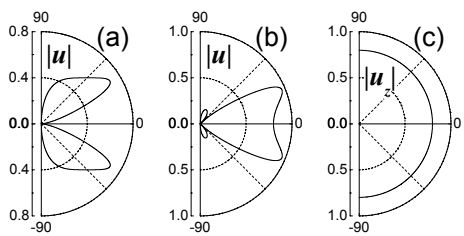


Fig. 3 Polar plots of displacement magnitude in far field (a) normal load, (b) tangential load, and (c) antiplane shear load for 2a=0.1 cm and f=500 Hz

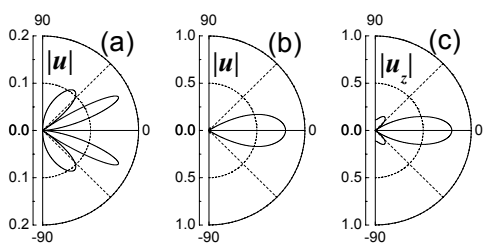


Fig. 4 Polar plots of displacement magnitude in far field under (a) normal load, (b) tangential load, and (c) antiplane shear load for 2a=1.0 cm and f=500 Hz.

sidelobes in the half space, but in Fig. 4(b) we can notice only one main lobe, because the sidelobes levels are less than 0.035. Under the present conditions, the strong beam of shear wave with the same far-field divergence $\theta_1$ is emitted forward from the tangential and antiplane shear load.

### 4.2 Wave Generation in Half Space Tissue

The displacements in half space were computed. The surface stress was assumed to be $\sigma_0/\mu = 1$, and a large value of $Q$ for the shear wave, i.e., $Q_s = Q_l = 354$, was used to observe the characteristics of wave generation in greater detail. Figs. 5 and 6 show the images of the magnitude of displacement generated by a vibration source of width 2a=0.1 cm and 1.0 cm, respectively. For the case of antiplane shear load, isocontours were drawn in black solid line to make it easy to identify the distribution of displacement. For the case of normal and tangential load, we can see relatively large displacements along the $x = 0$ surface due to the propagation of Rayleigh surface wave. The images obtained at 500 Hz in Figs. 5 and 6 are apparently similar to those in the far field as shown in Figs. 3 and 4, even though the region of interest is relatively close to the vibration source. On the other hand, the minimum frequency for which the sidelobes of shear wave start to appear when using the vibration source of width 0.1 cm and 1.0 cm are 2900 Hz and 290 Hz, respectively. Thus, when the width is 2a=0.1 cm, the two beam patterns at frequencies 200 Hz and 500 Hz are similar as can be seen in Fig. 5, because there are no additional sidelobes. Even in the case that the width of the vibration source with frequency 200 Hz increases by a factor of 10 to 2a=1.0 cm, the number of sidelobes does not increase.

Fig. 7 shows the angular distribution of displacement for several values of due to a

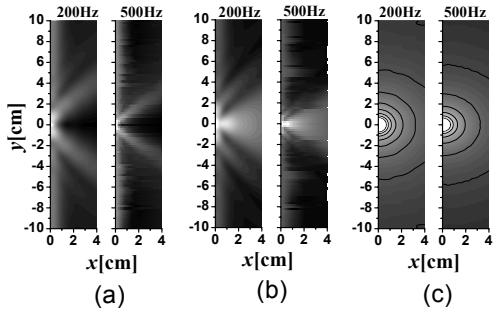


Fig. 5 Images of displacement magnitude to a vibration source of 2a=0.1 cm in half space due to (a) normal load, (b) tangential load, and (c) antiplane shear load

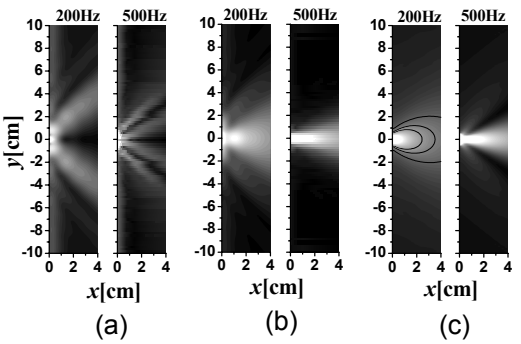


Fig. 6 Images of displacement magnitude to a vibration source of 2a=1.0 cm in half space due to (a) normal load, (b) tangential load, and (c) antiplane shear load

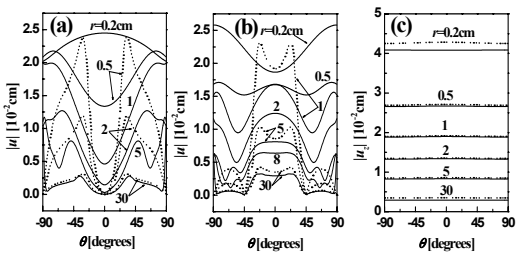


Fig. 7 Angular variation of displacement for various values of under (a) normal load, (b) tangential load, and (c) antiplane shear load for 2a==0.1 cm and f=200 Hz. The dotted lines represent results obtained using far field approximation

vibration source of width 2a=0.1 cm and frequency 200 Hz. Under normal and tangential load, there exists a relatively large displacement at the surface, $x=0$, i.e., in the vicinity of $\theta=90^\circ$ due to a Rayleigh surface wave. This surface displacement initially rapidly decreased with increasing distance from the vibration source along the surface, and slowly exponentially decreased beyond $y$=8 cm. The attenuation was nearly independent of the longitudinal acoustic $Q$, and was strongly dependent on the $Q_s$ value of the shear wave. A detailed analysis in a range $20 \le Q \le 354$ shows that the surface displacement decreases as $\exp[-\omega y/(2c_R Q_s)]$, where $c_R$ denotes the speed of the Rayleigh surface wave with the relationship $c_R \sim 0.95 c_s$. For the case of f=200 Hz and $Q_s$=354, the displacement magnitude at $y$=30 cm on the surface was $1.0\times10^{-2}$ cm under normal load and $0.55\times10^{-2}$ cm under tangential load. The magnitude decreased quite rapidly with increasing depth from the surface and at a depth of about 1.3 cm reached $e^{-1}$ of that at the surface. The depth is nearly identical to the wavelength of the Rayleigh surface wave, 1.38 cm.

Because for the normal load, $u_\theta = 0$ at $\theta = 0^\circ$ due to symmetry, the displacement around $\theta = 0^\circ$ shown in Fig. 7(a) is due to the contribution of the radial component, $u_r$. Although the displacement ratio $|u_\theta|/|u_r|$ in the far field is approximately $10^4$ with the radial displacement component relatively small, in the near field within a few centimeters from the vibration source the radial displacement component contributes significantly, unlike in the far field. Since the radial displacement component rapidly decreases with increasing distance from the vibration source, the shear wave is the main contributor in the whole region except for the surface area and approaches the displacement distribution in the far field. Another characteristic of the displacement under normal loading is that the angular location of the maximum displacement in the shear sidelobe, $\theta_{\max}$, depends on the distance, which is indicated in detail in Fig.

8(a). The angle $\theta_{\max}$ near the vibration source is significantly different from that in the far field approximation. The angle $\theta_{\max}$ decreases with increasing distance and tends to approach that in the far field. For low frequencies, the angle $\theta_{\max}$ approaches its asymptotic value slowly, but a little faster for high frequencies.

Under tangential load, the radial displacement $u_r$ related to the longitudinal wave is directed toward $45^\circ$ in the far field as shown in Fig. 2(b). It can be seen in Fig. 7(b) that the contribution of the radial displacement can be confirmed by the rapid decrease in displacement around $\theta = 55^\circ$ with increasing distance $r$. As in the case of normal load, though the longitudinal component affects the displacement distribution significantly, its influence rapidly decreases with increasing distance. At distances far from the vibration source, the shear displacement component becomes dominant, and the displacement ratio $|u_\theta|/|u_r|$ approaches about $10^7$. In the case of tangential load, if the width of the vibration source is smaller than the shear wavelength, in the far field approximation the displacement at $\theta = 45^\circ$ takes a minimum value of nearly zero. In the near field, however, the angle of minimum displacement, $\theta_{\min}$, is different from $\theta = 45^\circ$, which is indicated in detail in Fig. 8(b). As the vibration frequency increases, the angle $\theta_{\min}$ decreases more rapidly with distance, approaching $45^\circ$ in the far field. The distance where the angle of minimum displacement approaches $45^\circ$ represents the point where the angular distribution of displacement begins to agree well with the far field approximation. It is about 26 cm for 200 Hz.

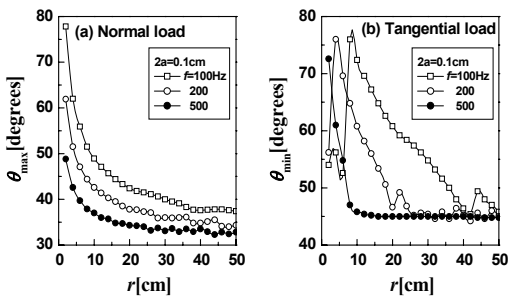


Fig. 8 (a) Variation of the angle $\theta_{\max}$ of maximum displacement in the shear sidelobe generated by a normal load as a function of distance $r$. (b) Variation of the angle $\theta_{\min}$ of minimum displacement due to a tangential load as a function of distance $r$

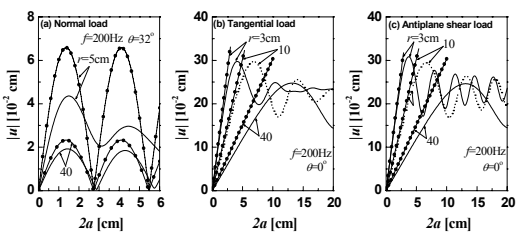


Fig. 9 Variation of displacement magnitude versus the width of vibration source for various values of $r$ under (a) normal load, (b) tangential load, and (c) antiplane shear load. The solid lines with circles represent results obtained using far field approximation

Under antiplane shear load, Rayleigh surface and longitudinal waves are not generated, but only shear wave is emitted. We can see in Fig. 7(c) that under antiplane shear loading the displacement distribution near the vibration source is nearly the same as that in the far field and that only its magnitude decreases with increasing distance from the vibration source.

Fig. 9 shows the dependence of displacement magnitude on the width of the vibration source at a given point in half space. Here, the frequency of the vibration source is 200 Hz. Because the displacement under normal load was calculated at $\theta$=32° which is away from the vibration axis, the displacement in the far field varies as the term, $\sin(k_s a \sin\theta)$, in the numerator of eqn. (9) for component $u_\theta$. The displacement component $u_\theta$ in the far field continues to increase as the source width increases until it reaches $2a = c_s/(2f\sin\theta)$, and becomes zero at $2a = nc_s/(f\sin\theta)$, $n = 1, 2, 3, \ldots$. When $\theta$=32° and f=200 Hz, the displacement in

the far field increases until the width of the vibration source reaches 2a=1.37 cm, and becomes almost zero at 2a=2.74, 5.47 cm, etc. Fig. 9(a) shows that the displacement at $r=$ 40 cm and that in the far field are similar. However, the displacement at a near distance of $r=5$ cm is different from that in the far field in terms of displacement magnitude and locations of local minima. This indicates that because several wave modes with comparable amplitudes, such as the longitudinal, shear, and surface waves, are superposed in the near distance region as shown in Figs. 7(a) and 8(a), the displacement distribution cannot be accurately represented using the far field approximation where the shear wave contributes predominantly.

The displacements along the axis ($\theta$=0°) in areas where the width of the vibration source is narrow under tangential and antiplane shear loading, shown in Figs. 9(b) and (c), respectively, have a tendency similar to the far field approximation, and increases almost linearly. After reaching the maximum, the displacement starts to oscillate as the width 2a increases. The range of 2a in which the displacement monotonically increases becomes larger with increasing distance. The monotonically increasing range can be approximately explained by the near field length $N$, which distinguishes the on-axis displacement of the vibration source as belonging to the near or far field. The displacement magnitude fluctuates with distance along the axis of the vibration source at distances less than $N$, while it decreases monotonically at distances larger than $N$[31]. Since the propagation of shear wave in tissue is dominant for the low frequency range that we consider at present, the near field distance $N_s$ for shear wave is used for range determination. Since $N_s$ is approximately equal to $a^2 f/c_s$, the width of the vibration source for which an observation point $r$ on the axis of the vibration source is larger than $N_s$ is in the range between 0 and $W$, where $W$ is approximately $\sqrt{4c_s r/f}$. $W$ is given as 4.17, 7.62, and 15.23 cm for $r$=3, 10, and 40 cm, respectively. If the width of the vibration source is less than, the given position $r$ becomes farther than $N_s$, and the displacement increases with 2a, as is the case with the far field approximation. In contrast, if the source width is larger than $W$, the displacement oscillates with increasing 2a similarly to the behavior of the near field because $r$ is smaller than $N_s$. The behavior of the on-axis displacement, which depends on the source width, can be more clearly observed in Fig. 9(c). This is because the fluctuation characteristics of the on-axis displacement appear clearly in the region where $r<N_s$ due to the generation of only shear wave under antiplane shear loading. Under tangential loading, however, the oscillation of the displacement is not quite apparent at $r$=3 cm. As we have seen above, this reflects the fact that under tangential loading, the oscillation of the one-axis displacement in the near distance range is not quite apparent because displacements related to various wave modes are superposed.

### 4.3 Vibration Pattern in Single Layer and Finite-Sized Tissue

The displacements in a single-layer tissue of infinite plate type were computed using eqns. (5) and (15). The thickness of the layer was $L$ =4 cm. It was assumed that $\sigma_{0/}\mu=1$ and $Q_l=Q_s=354$ as before. Fig. 10 shows the displacement pattern formed by a vibration source of width 1.0 cm. The wave generated by the vibration source together with multiple waves reflected from the two boundaries forms an interference pattern.

From the images obtained at 500 Hz for normal and antiplane shear load, we can clearly

see that the sidelobe parts are reflected from the boundaries and propagate along the $y$ axis direction. We can see the interference pattern more prominent under the tangential and antiplane shear load, in which the reflected waves are strongly superposed, rather than under the normal load, in which the shear wave propagates in a shape resembling the letter V.

A guided wave is generated in the single-layer medium due to the vibration source, and $\xi$ in eqns. (5) and (15) is the wave number of the guided wave propagating in the $y$ direction. The dispersion relation is obtained from the condition that makes the denominator of the displacement expression equal to zero. The cutoff frequencies of guided wave modes determined from $\xi = 0$ in the dispersion relationship correspond to thickness resonant frequencies, and the thickness resonance condition of shear waves is $\cos(\omega L/c_s) = 0$ considering that the medium is elastic $(Q \to \infty)$. Therefore, the thickness resonant frequencies are given as $f_m = mc_s/4L$ $(m = 1, 3, 5, ...)$. Because the frequency of 200 Hz is very close to the resonant frequency, f=199.38 Hz, the amplitude of the interference pattern significantly increases, generating a prominent interference pattern in the images obtained at 200 Hz in Fig. 10(b) and (c). The wavelength of the 200 Hz shear wave is 1.45 cm. Because there can be 5.52 half wavelengths in $L$=4 cm, there are about 5.5 bright strips in the $x$ axis direction.

The frequency 500 Hz is slightly different from the resonant frequency $f_{27}$=489.38 Hz, and the amplitude of the interference patterns is relatively small. The beam emitted from the vibration source is buried in the interference pattern whose amplitude is large due to resonance as shown in the images of Fig. 10(b) and (c) obtained at 200 Hz. However, in the images obtained at 500 Hz, where the amplitude of the interference pattern is small, some reflection of emitted sidelobes can be observed. Because

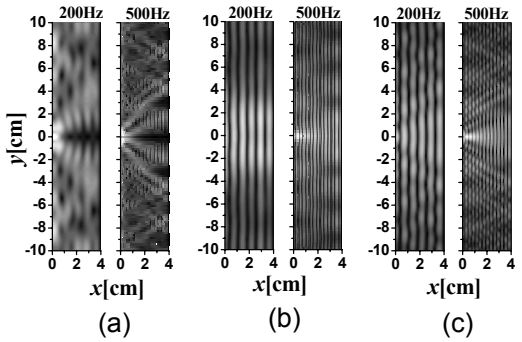


Fig. 10 Images of displacement magnitudes for various types of loads, all of width 2a= 1.0 cm, in an infinite plate under (a) normal load, (b) tangential load, and (c) antiplane shear load

the wavelength of the 500 Hz shear wave is 0.58 cm and $L$=4 cm corresponds to 13.79 half wavelengths, in the images of Fig. 10 obtained at 500 Hz, we can observe 13.5 bright strips.

Shown in Figs. 11 and 12 are the characteristics of the change in displacement magnitude in the single layer as a function of the frequency of the vibration source. The displacements were computed at point $(x,y)$ =(2 cm, 2.5 cm), or $(r,\theta)$=(3.202 cm, 51.340°), and the width of the vibration source was set to 1.0 cm. The dependence of the displacement on the frequency in the half space as well as in the far field is also shown in Figs. 11 and 12. The locations of the thickness resonant frequencies, $f_7$ to $f_{27}$, are indicated in the displacement curve for the normal load in Fig. 11. The displacement in the far field periodically repeats increases and decreases due to the presence of the term, $\sin(k_s a \sin\theta)$, in the numerator of the expression for component $u_\theta$, and becomes almost zero at frequencies, $f = nc_s/(2a\sin\theta)$ $= n \times 371.38$ Hz $(n = 1, 2, 3, ...)$.

As we have seen in Fig. 7(c), under antiplane shear loading, the displacement in the half space agrees quite well with that in the far field. The displacement in the infinite plate takes the form of that in the half space plus the

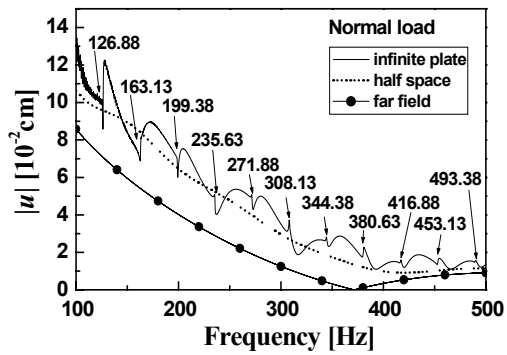


Fig. 11 Variation of displacement magnitudes versus frequency at x=2 cm and y=2.5 cm under normal load for 2a=1.0 cm. The numbers above the curves indicate the thickness resonant frequencies(Hz)

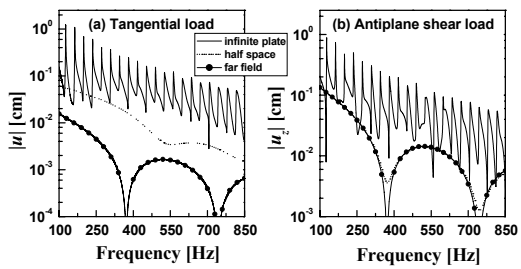


Fig. 12 Variation of displacement magnitudes versus frequency at x=2 cm and y=2.5 cm under (a) normal load and (b) antiplane shear load for 2a=1.0 cm

resonance effect. This is because the multiple reflected waves from boundaries are superimposed on the wave emitted from the vibration source. The displacement images in Fig. 10 clearly demonstrate this fact. The resonance behavior is more pronounced for the tangential and antiplane shear load where most of the shear wave propagates in front of the vibration source.

Figs. 13 and 14 show the vibration pattern formed by a vibration source of width 2a =1.0 cm in a finite-sized tissue of size $L\times H$= 4 cm×10 cm. In order to be able to observe closely the interference pattern formed by the presence of four boundaries, we computed the displacement magnitude by assuming the $Q$ value is large so that the shear wave is not severely attenuated ($Q_s = Q_l$ =354), with the resulting displacements shown in Fig. 13. Fig. 14 represents the images of displacement magnitudes obtained using a small value of shear acoustic $Q$($Q_s$=20) to show the effects of the attenuation on shear waves in real tissue. Although not much is known about the value of $Q$ in tissue, the $Q_s$ values used here are within the approximate range (3 to 100) of $Q$ values estimated from the energy loss in soft tissue and tissue-mimicking phantom available in the literature[11,14,32-35]. We can see the vibration pattern in Fig. 13 is more complicated than that in Fig. 10 (the case of infinite plate) due to the presence of the boundaries, $y=\pm H/2$.

While it is not a trivial task to analyze the in-plane vibration in a finite-sized medium, the resonant frequency can be found easily for antiplane shear load in which no mode conversion occurs in reflection because only the shear wave is generated. The condition for excitation of a guided horizontal shear wave in a single layer is given as $\cos\beta' L = 0$ $(\beta = i\beta')$, i.e., $\omega^2/c_s^2 = \xi^2 + (m\pi/2L)^2$ $(m = 1,3,5,...)$. The resonance condition in the $y$ direction, in which the surfaces $y=\pm H/2$ are free boundaries, is given as $\xi = l\pi/H$ $(l = 0,1,2,...)$[24]. The mode is symmetric with respect to $y$ if $l$ is even and antisymmetric with respect to $y$ if $l$ is odd. Therefore, the resonant frequency for the $(m,l)$ mode is expressed as $f_{m,l} = (c_s/2)[(m/2L)^2 + (l/H)^2]^{1/2}$. Because the present case corresponds to a forced vibration in which an antiplane shear load, which is symmetric about $y$=0, is applied, only symmetric modes are excited. In Fig. 13(c), the mode (9,8) is excited because 200 Hz is very close to $f_{9,8}$=200.16 Hz. However, because 500 Hz lies between $f_{27,6}$ =497.05 Hz and $f_{27,8}$=502.94 Hz, conspicuous modal patterns are not formed.

When a clearly noticeable salient interference pattern between shear waves is formed in the $x$

axis direction for the tangential load as in Fig. 13(b), the number of bright strips in the $y$ direction can be determined by estimating the wavelength of the guided wave from the relationship, $\beta' = (\omega^2/c_s^2 - \xi^2)^{1/2}$, between the wave number $\beta'$ in the $x$ axis direction and the wave number $\xi$ of the guided wave. The relationship between the wavelength $\lambda_x$ in the $x$ direction and the wavelength $\lambda_y$ in the $y$ direction is given by $1/\lambda_y^2 = (f/c_s)^2 - 1/\lambda_x^2$. For the case of using 200 Hz, the number of bright strips is about 5.5 in the $x$ direction, leading to $\lambda_x$~1.4545 cm and $\lambda_y$~18.3556 cm, and the number of bright strips in the $y$ direction is 1, considering the fact that the height, $H$=10 cm, is about as long as the half wavelength $\lambda_y/2$. For the case of 500 Hz, the number of bright strips is about 13.5 in the direction, leading to $\lambda_x$~0.5926 cm and $\lambda_y$~2.8285 cm, and the number of bright strips in the $y$ direction is 7, considering the fact that the height, $H$=10 cm, is seven times as long as the half wavelength $\lambda_y/2$.

We can confirm in Fig. 14 that the reflection effect at the surfaces, $y = \pm H/2$, has been greatly reduced due to the relatively large attenuation of a shear wave. For the case of normal load with a vibration frequency of 200 Hz, the shear wave is emitted directly toward the surfaces, $y = \pm H/2$. Thus, the effect of reflection is rather significant here, but becomes almost unnoticeable when the frequency is increased to 500 Hz, due to an increase in attenuation. For the case of tangential and antiplane shear load where the shear wave propagates predominantly away from the front of the vibration source, the interference pattern is mostly due to reflections occurring at the surface $x = L$. Despite the interference, since its effect is greatly diminished, the beam patterns emitted from the vibration source are relatively well manifested compared to those in the half space(Fig. 6).

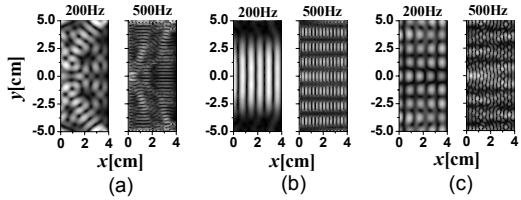


Fig. 13 Images of displacement magnitudes under various types of loads, all of width 2a=1.0 cm, in a finite-sized plate under (a) normal load, (b) tangential load, and (c) antiplane tangential load. $Q_l$= $Q_s$=354

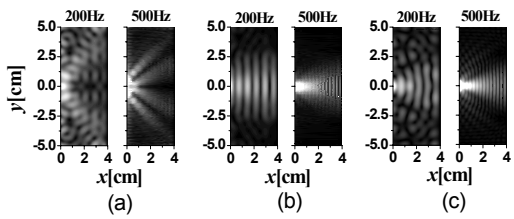


Fig. 14 Images of displacement magnitudes under various types of loads, all of width 2a=1.0 cm, in a finite-sized plate under (a) normal load, (b) tangential load, and (c) antiplane tangential load. $Q_l = 354$, $Q_s = 20$

## 5. Conclusions

We have investigated beam and vibration patterns generated when soft tissue is subjected to low-frequency normal, tangential, and antiplane shear loading. To this end, displacements are computed in half space, single layer, and finite-sized tissue, and some results for vibration generation in soft tissue are presented.

The characteristics of displacement generated in half space from a surface vibration source are explored, and the distribution of displacement in the near field is compared to that in the far field and analyzed. Under normal and tangential loading, the angular distribution of displacement within a few centimeters from the vibration source is found to differ from that in the far field because the several types of waves, all of which have comparable amplitudes, are added together. A large amplitude surface wave is generated, and its displacement is found to

attenuate along the surface depending on the shear acoustic *Q*. The shear wave mainly propagates inside tissue because of the large longitudinal-to-shear wave speed ratio. In the case of plane strain, the distribution of displacement due to antiplane shear loading that generates only a pure shear wave agrees well with that obtained from the far field approximation over the entire region including the vicinity of the vibration source.

By computing the displacement in tissues of infinite plate type as well as finite dimensions, the process that waves emitted from a surface vibration source construct vibration patterns is explained in detail. Tissue boundaries are found to exert an effect on the vibration pattern in tissue by superimposing interference patterns caused by multiple reflections to the beam pattern emitted from the vibration source. If vibration is excited in tissue at near the resonance frequency, the amplitude of interference pattern increases significantly, burying the emitted beam pattern inside of it. The interference pattern in plate and rectangular tissue is more pronounced under tangential and antiplane shear loading than under normal loading. Although the shear wave plays a dominant role in the displacement of soft tissue for all types of vibration sources considered, even at the same vibration excitation frequency the vibration pattern in finite-sized tissue differs depending on the type of vibration source. It is expected that investigation into vibration characteristic in tissue will provide fundamental information that helps to interpret vibration generation and acquired image in elasticity imaging such as sonoelastography.

## Acknowledgement

This work was supported by the R&D program of MKE/KEIT (10033627, Ultrasound Imaging Technique of Tissue Elasticity).

## References

[1] S. Catheline, F. Wu and M. Fink, "A solution to diffraction biases in sonoelasticity: The acoustic impulse technique," *J. Acoust. Soc. Am.*, 105(5), pp. 2941-2950 (1999)

[2] K. J. Parker, S. R. Huang, R. A. Musulin and R. M. Lerner, "Tissue response to mechanical vibrations for sonoelasticity imaging," *Ultrasound Med. Biol.*, 16(3), pp. 241-246 (1990)

[3] K. J. Parker, L. S. Taylor and S. Gracewski, "A unified view of imaging the elastic properties of tissue," *J. Acoust. Soc. Am.*, 117(5), pp. 2705-2712 (2005)

[4] S. F. Levinson, M. Shinagawa and T. Sato, "Sonoelastic determination of human skeletal muscle elasticity," *J. Biomechanics*, 28(10), pp. 1145-1154 (1995)

[5] M. Fatemi and J. F. Greenleaf, "Probing the dynamics of tissue at low frequencies with the radiation force of ultrasound," *Phys. Med. Biol.*, 45, pp. 1449-1464 (2000)

[6] T. Varghese, J. A. Zagzebski, P. Rahko and C. S. Breburda, "Ultrasonic imaging of myocardial strain using cardiac elastography," *Ultrasonic Imaging*, 25(1), pp. 1-16 (2003)

[7] C. L. de Korte and A. F. W. Van der Steen, "Intravascular ultrasound elasto-graphy: an overview," *Ultrasonics*, 40, pp. 859-865 (2002)

[8] Y. Yamakoshi, J. Sato and T. Sato, "Ultrasonic imaging of internal vibration of soft tissue under forced vibration," *IEEE Trans. Ultrason. Ferroelect. Freq. Contr.*, 37(2), pp. 45-53 (1990)

[9] L. Sandrin, M. Tanter, S. Catheline and M. Fink, "Shear modulus imaging using 2-D transient elastography," *IEEE Trans. Ultrason. Ferroelect. Freq. Contr.*, 49(4),

426-435 (2002)

[10] J. Bercoff, S. Chaffai, M. Tanter, L. Sandrin, S. Catheline, M. Fink, J. L. Gennisson and M. Meunier, "In vivo breast tumor detection using transient elastography," *Ultrasound Med. Biol.*, 29(10), pp. 1387-1396 (2003)

[11] K. J. Parker, D. Fu, S. M. Gracewski, F. Yeung and S. F. Levinson, "Vibration sonoelasticity and the detectability of lesions," *Ultrasound Med. Biol.*, 24(9), pp. 1437-1447 (1998)

[12] S. Catheline, J. L. Thomas, F. Wu and M. A. Fink, "Diffraction field of a low frequency vibrator in soft tissues using transient elastography," *IEEE Trans. Ultrason. Ferroelect. Freq. Contr.*, 46(4), pp. 1013-1019 (1999)

[13] D. Fu, S. F. Levinson, S. M. Gracewski and K. J. Parker, "Non-invasive quantitative reconstruction of tissue elasticity using an iterative forward approach," *Phys. Med. Biol.*, 45, pp. 1495-1510 (2000)

[14] L. Gao, K. J. Parker and S. K. Alam, "Sonoelasticity imaging: Theory and experimental verification," *J. Acoust. Soc. Am.*, 97(6), pp. 3875-3886 (1995)

[15] Z. Wu, L. S. Taylor, D. J. Rubens and K. J. Parker, "Shear wave focusing for three-dimensional sonoelastography," *J. Acoust. Soc. Am.*, 111(1), pp. 439-446 (2002)

[16] Z. Wu, L. S. Taylor, D. J. Rubens and K. J. Parker, "Sonoelastographic imaging of interference patterns for estimation of the shear velocity of homogeneous biomaterials," *Phys. Med. Biol.*, 49, pp. 911-922 (2004)

[17] Z. Wu, K. Hoyt, D. J. Rubens and K. J. Parker, "“Sonoelastographic imaging of interference patterns for estimation of the shear velocity distribution in biomaterials," *J. Acoust. Soc. Am.*, 120(1), pp. 535-545 (2006)

[18] J. McLaughlin, D. Renzi, K. Parker and Z. Wu, "Shear wave speed recovery using moving interference patterns obtained in sonoelastography experiments," *J. Acoust. Soc. Am.*, 121(4), pp. 2438-2446 (2007)

[19] K. Hoyt, B. Castaneda and K. J. Parker, "Two-dimensional sonoelastographic shear velocity imaging," *Ultrasound Med. Biol.*, 34(2), pp. 276-288 (2008)

[20] T. J. Royston, H. A. Mansy and R. H. Sandler, "Excitation and propagation of surface waves on a viscoelastic half-space with application to medical diagnosis," *J. Acoust. Soc. Am.*, 106(6), pp. 3678-3686 (1999)

[21] E. M. Timanin, "Displacement field produced by a surface source of vibrations in a layered biological tissue," *Acoust. Phys.*, 48(1), pp. 98-104 (2002)

[22] B. N. Klochkov, "Near field of a low-frequency source of forced vibration on a layered biological tissue," *Acoust. Phys.*, 48(1), pp. 70-76 (2002)

[23] J. N. Barshinger and J. L. Rose, "Guided wave propagation in an elastic hollow cylinder coated with a viscoelastic material," *IEEE Trans. Ultrason. Ferroelect. Freq. Contr.*, 51(11), pp. 1547-1556 (2004)

[24] K. F. Graff, "Wave Motion in Elastic Solids," Ohio State University Press (1975)

[25] J. D. Achenbach, "Wave Propagation in Elastic Solids," North-Holland, Amsterdam, (1975)

[26] B. A. Auld, "Acoustic Fields and Waves in Solids," John Wiley & Sons, New York, 1973.

[27] B. Angelsen, "Ultrasound Imaging: Waves, Signals and Signal Processing," Emantec, Trondheim, Norway, (2000)

[28] L. Sandrin, B. Fourquet, J. M. Hasquenoph, S. Yon, C. Fournier, F. Mal, C. Christidis and M. Ziol, "Transient elastography: A new noninvasive method

for assessment of hepatic fibrosis," *Ultrasound Med. & Biol.*, 29(12), pp. 1705-1713 (2003)

[29] A. P. Sarvazyan, O. V. Rudenko, S. D. Swanson, J. B. Fowlkes and S. Y. Emelianov, "Shear wave imaging: A new ultrasonic technology of medical diagnostics," *Ultrasound Med. Biol.*, 24(9), pp. 1419-1435 (1998)

[30] K. Nightingale, S. McAleavey and G. Trahey, "Shear-wave generation using acoustic radiation force: In vivo and ex vivo results," *Ultrasound Med. Biol.*, 29(12), pp. 1715-1723 (2003)

[31] L. E. Kinsler, A. R. Frey, A. B. Coppens and J. V. Sanders, "Fundamentals of Acoustics," John Wiley & Sons, New York, (1982)

[32] J. Bercoff, M. Tanter, M. Muller and M. Fink, "The role of viscosity in the impulse diffraction field of elastic waves induced by the acoustic radiation force," *IEEE Trans. Ultrason. Ferroelect. Freq. Contr.*, 51(11), pp. 1523-1536 (2004)

[33] C. S. Chu and M. C. Lee, "Finite element analysis of cerebral contusion," *Advances in Bioengineering*, ASME-BED-Vol. 20, pp. 601-604 (1991)

[34] M. Hauth, J. Gross, W. Strasser and G. F. Buess, "Soft tissue simulation based on measured data," *Proceedings of the 6th International Conference on Medical Image Computing and Computer-Assisted Intervention (MICCAI 2003)*, Montreal, Canada, 262-270 (2003)

[35] C. R. Hou, "Design and development of a pulsed wave Doppler ultrasonic system for measuring the viscoelasicity of soft tissue," Ph. D. Dissertation, National Cheng Kung University, Taiwan (2002)